RP Current Trends In Applied Sciences (e-ISSN: 2583-7486)
Vol. 5, No. 1 (January – March 2026) pp. 1–10

RESEARCH PLATEAU PUBLISHERS

Cite this article: C.R. Eldin Jeeva, A. Selvaraj, Unsteady ferro-nanofluid flow with variable concentration over an inclined riga plate under MHD, radiation, chemical reaction, and bioconvection embedded in a porous medium, *RP Cur. Tr. Appl. Sci.* **5** (2026) 1–10.

Original Research Article

Unsteady ferro-nanofluid flow with variable concentration over an inclined riga plate under MHD, radiation, chemical reaction, and bioconvection embedded in a porous medium

C.R. Eldin Jeeva*, Dr. A. Selvaraj

Vels Institute of Science, Technology and Higher Studies, Chennai, Tamil Nadu, India
*Corresponding author, E-mail: jeevaonline@gmail.com

ARTICLE HISTORY
Received: 23 Feb. 2026
Revised: 27 May 2026
Accepted: 27 May 2026
Published: 12 June 2026

KEYWORDS
Ferro nanofluid;
Lorentz force;
Micororganism;
Buoyancy.

ABSTRACT
This paper presents an exact analytical investigation of unsteady variable concentration ferro-nano fluid flow past an inclined plate under the combined effects of thermal and solutal buoyancy, magnetic field interaction and bioconvection due to motile microorganisms. The governing system of equation accounts for Lorentz forces arising from an exponentially decaying magnetic field, porous medium resistance, thermal radiating and chemical reaction effects. Closed form solutions for the velocity, temperature, concentration and microorganism density distributions are obtained using the Laplace transform technique. The results elucidate the coupled influence of buoyancy forces, magnetization and bioconvective mechanisms on ferro-nanofluid transport characteristics. The outcomes provide useful insights for the design and optimization of magnetohydrodynamics and bio-thermal systems involving ferro-nanofluids.

1. Introduction

Ferro-nanofluids are advanced engineered fluids formed by suspending magnetic nanoparticles such as Fe_3O_4 in a conventional base fluid, which enables simultaneous enhancement of thermal conductivity and active control of fluid motion through externally applied magnetic fields. Due to magnetic field interaction and magnetized nanoparticles, ferro-nanofluids exhibit unique magneto-hydrodynamic and heat transfer characteristics that significantly influence momentum, thermal, and mass transport processes. Electronic cooling systems, heat exchangers, magnetic sealing, targeted drug delivery, biomedical devices, energy conversion technologies, microfluidic systems, and aerospace thermal management use these fluids, which have received attention. In practical engineering situations, ferro-nanofluid flows often occur under unsteady conditions and are affected by additional mechanisms such as thermal radiation, chemical reactions, porous media, and bioconvection induced by motile microorganisms, further modifying the transport behavior. Consequently, the theoretical and mathematical analysis of ferro-nanofluid flow is crucial in understanding combined effects of magnetic forces as well as thermal phenomena, thereby contributing to the efficient design and optimization of modern magnetically controlled thermal systems.

"Magnetohydrodynamic parabolic flow" via "an accelerated isothermal vertical plate with heat and mass diffusion under rotating forces has been assessed by Selvaraj et al. [1]. Lakshmikaanth et al. [2] assessed how Hall current, internal heat generation affect MHD flow over an isothermal vertical plate subjected to chemical reaction and thermal radiation. Radiation decreased fluid velocity and heat enhanced it. Kesavaiah and Jahagirdar [3] studied MHD flow radiation absorption and chemical reactions on an exponentially accelerated inclined porous plate. Unsteady MHD flow via inclined permeable plate in a porous media was impacted by thermos diffusion, radiation, and chemical reaction, according to Prabhakar Reddy et al. [4]. Chemical reaction increases "Sherwood number," while radiation parameter and duration increase "Nusselt number." Krishna et al. [5] evaluated radiation absorption impact on MHD nanofluid flow across vertically moving absorbent plate. Radiation parameter raised velocity and temperature. Das et al. [6] studied thermal radiation on nanofluid over vertical plate, whereas Prasad et al. [7] observed increased velocity, temperature, and skin friction in MHD nanofluid flow with radiation absorption. Agarwall and Ahmed [8] examined "MHD mass transfer flow" over an inclined plate with variable temperature in a porous medium, while Krishna and Chamkha [9] studied" Hall effects of water-based nanofluid flow. Hayat et al. [10] showed that increasing magnetic parameter decreases velocity field in nanofluid flow caused by conductive heating on a Riga plate.

Further studies incorporating radiation, chemical reaction, and bioconvection have been reported extensively. Prakash et al. [11] assessed mass transfer and radiative heat in unsteady "MHD Casson fluid flow," while Raghunath et al. [12] observed that Jeffrey and suction parameters decrease velocity "as chemical reaction impacts on Jeffrey nanofluid flow over inclined vertical plate under radiation. As variable viscosity increases, Afridi et al. [13] discovered velocity drop in second law analysis of dissipative flow over a Riga plate with "nonlinear Rosseland radiation." Reddy and Rao [14] discovered increased Prandtl number and radiation-thinning

thermal boundary layers in unsteady MHD flow on a porous vertical plate. Rana et al. [15] explored Hall current and Lorentz force effects on inclined Riga plate flow, whereas Arthur et al. [16] found magnetic effects suppressed chemically reactive "Casson fluid flow" across a porous surface. Wang et al. [17]" executed computational assessment of bioconvection in Prandtl nanofluid flow and revealed that intensified magnetic and porosity impacts limit fluid velocity. Bioconvection in MHD micropolar nanofluid flow over a stretched sheet has been assessed by Farooq et al. [18], who examined that velocity increased as magnetic field intensity increased. Several other investigations addressed unsteady micropolar nanofluids [19], radiative riga plate flows [20], accelerated vertical plate problems [21], viscous dissipation with thermal radiation [22], chemically reactive Riga plate flows [23], modified nanofluid transport over Riga surfaces [24], nanofluid bioconvection with gyrotactic microroganisms [25], hybrid nanofluids with chemical reactions [26], Arrhenius activation energy effects [27], classical MHD nanofluid convection [28], microorganism-driven transport phenomena [29]-[32], and chemically reactive unsteady MHD flows [33], [34].

Despite the extensive contributions, an exact analytical treatment of unsteady ferro-nanofluid flow over an inclined Riga plate incorporating variable concentration, bioconvection, radiation, and chemical reaction under an exponentially decaying magnetic field remains unexplored. This paper fills this gap by creating a novel analytical framework utilizing "Laplace transform technique" to produce closed-form velocity, temperature, concentration, and microbe density distribution solutions. Detailed graphs describe impact of altering "physical parameters and engineering numbers" like skin friction coefficient, Sherwood number, Nusselt number, and bioconvective number. Results formulate the first benchmark dataset for ferro-nanofluid flow problems and highlight novel interactions between magnetic forcing, radiative heat transfer, chemical reaction, and bioconvective transport along an inclined Riga plane.

2. Mathematical formulation of the problem

Unstable, incompressible ferro-nanofluid free-convection across an inclined vertical Riga plate is studied. Plate tilted at α to vertical. Coordinate system aligns x-axis with plate and normalizes y-axis. Transversely, B_0 uniform magnetic field is applied. Ferro nano fluid is assumed to contain motile microorganisms, which induce bioconvection within the flow field. Initially, $t \leq 0$, plate and fluid maintain a homogeneous ambient temperature T_∞, nanoparticle concentration C_∞ and microbe density N_∞. Riga plate generates a "tangential Lorentz force" which acts upon fluid near the plate. This electromagnetic forcing is incorporated into the momentum equation as an additional body force term, which decays exponentially with the normal distance from the plate. For $t > 0$, plate temperature, nanoparticle concentration, and microorganism density are suddenly increased to T_w, C_w and N_w. As a result, thermal, solutal, and bioconvective boundary layers develop along plate. All physical parameters are independent of x if plate is infinite in "x-direction," and velocity component normal to the plate is ignored. Under these assumptions, the governing equations reduce to one dimensional, time-dependent system, which is formulated as follows.

Momentum equation:

$$\frac{\partial u}{\partial t} = \frac{\mu_{nf}}{\rho_{nf}}\frac{\partial^2 u}{\partial y^2} + g\beta_T(T - T_\infty)sin\alpha + g\beta_C(C - C_\infty)sin\alpha - g\beta_N(N - N_\infty)sin\alpha + \frac{\sigma B_0^2}{\rho_{nf}}(u_0 e^{-ky} - u) - \frac{u\mu_{nf}}{\rho_{nf}K^*} + \frac{\mu_0}{\rho_{nf}}\frac{\partial(MH)}{\partial y} \quad (1)$$

Temperature equation:

$$\frac{\partial T}{\partial t} = \frac{k_{nf}}{\rho_{nf}C_{p,nf}}\frac{\partial^2 T}{\partial y^2} - \frac{1}{\rho_{nf}C_{p,nf}}\frac{\partial q_r}{\partial y} \quad (2)$$

Concentration equation:

$$\frac{\partial C}{\partial t} = D_{nf}\frac{\partial^2 C}{\partial y^2} - k_t(C - C_\infty) \quad (3)$$

Bioconvection equation:

By neglecting the chemotactic and gyrotactic drift in comparison with random motility, the microorganism distribution may be expressed through the simplified bioconvection equation

$$\frac{\partial N}{\partial t} = D_m\frac{\partial^2 N}{\partial y^2} \quad (4)$$

The Magnetic body force term $\frac{\partial(MH)}{\partial y}$ is evaluated by assuming a linearly magnetizable ferrofluid, for which the magnetization is proportional to the applied magnetic field and is given by $M = \chi H$. The applied magnetic field is modelled as an exponentially decaying function of the normal coordinate $H = H_0 e^{-\lambda y}$, representing the realistic attenuation of magnetic field intensity away from the Riga plate. Substituting these relations into the magnetic body force term yields a spatially varying Lorentz force. Consequently, the momentum equation governing the flow reduces to

$$\frac{\partial u}{\partial t} = \frac{\mu_{nf}}{\rho_{nf}}\frac{\partial^2 u}{\partial y^2} + g\beta_T(T - T_\infty)sin\alpha + g\beta_C(C - C_\infty)sin\alpha - g\beta_N(N - N_\infty)sin\alpha + \frac{\sigma B_0^2}{\rho_{nf}}(u_0 e^{-ky} - u) - \frac{u\mu_{nf}}{\rho_{nf}K^*} - \frac{\mu_0}{\rho_{nf}}2\lambda\chi H^2{}_0 e^{-2\lambda y} \quad (5)$$

The Rosseland diffusion approximation, which works for optically thick media, is used to model radiative heat flow within ferro-nanofluid. Under this assumption. The expression for the "radiation heat flux" is

$q_r = -\frac{4\sigma^*}{3k}\frac{\partial}{\partial y}(T^4)$

Here, $\sigma*$ represents Stefan-Boltzmann constant, k represents mean absorption coefficient.

Assuming small temperature variations across flow, fourth-power temperature term T^4 is linearized by performing "Taylor series expansion" about $T_\infty$and neglecting higher-order terminology, resulting i

$T^4 \approx 4T_\infty^3 T - 3T_\infty^4$

Thus $\frac{\partial q_r}{\partial y} = -\frac{16\sigma}{3k}T_\infty^3\frac{\partial^2 T}{\partial y^2}$

Hence, the Temperature equation is

$$\frac{\partial T}{\partial t} = \frac{k_{nf}}{\rho_{nf}C_p}\frac{\partial^2 T}{\partial y^2} + \frac{1}{\rho_{nf}C_p}\frac{16\sigma}{3k}T_\infty^3\frac{\partial^2 T}{\partial y^2} \quad (6)$$

Initial and the boundary "conditions are:

For $\forall t \le 0\ u = 0, T = T_\infty, C = C_\infty, N = N_\infty$

For $t > 0, u = u_0, T = T_w, C = C_\infty + (C_w - C_\infty)At, N = N_w$ at $y = 0$

At $y \to \infty, u = 0, T \to T_\infty$, $C \to C_\infty$, $N \to N_\infty$, Where $A = \frac{\vartheta_{nf}}{L^2}$

Introducing the non-dimensional parameter

$U = \frac{uL}{\vartheta_{nf}}$, $t_1^* = \frac{t\vartheta_{nf}}{L^2}$, $Y = \frac{y}{L}, \theta = \frac{T-T_\infty}{T_W-T_\infty}, \varphi = \frac{C-C_\infty}{C_W-C_\infty}$, $n = \frac{N-N_\infty}{N_W-N_\infty}$

$GT = \frac{g\beta_T(T-T_\infty)L^3}{{\vartheta_{nf}}^2}$, $GC = \frac{g\beta_C(C-C_\infty)L^3}{{\vartheta_{nf}}^2}$, $Gn = \frac{g\beta_N(N-N_\infty)L^3}{{\vartheta_{nf}}^2}$, $M = \frac{\sigma B_0^2}{\rho_{nf}\vartheta_{nf}}L^2$, $D\alpha = \frac{K^*}{L^2}$,

$Fm = \frac{2\mu_0\lambda\chi H_0^2 L^3}{\rho_{nf}{\vartheta_{nf}}^2}$, $Prnf = \frac{\rho_{nf}C_{p,nf}}{k_{nf}}$, $Rd = \frac{16\sigma}{3kk_{nf}}T_\infty^3$, $Sc = \frac{D_{nf}}{\vartheta_{nf}}$, $Kc = \frac{K_t L^2}{\vartheta_{nf}}$, $Scm = \frac{D_m}{\vartheta_{nf}}$.

Then the equations (5), (6) (3) and (4) reduces to

$\frac{\partial U}{\partial t_1^*} = \frac{\partial^2 U}{\partial Y^2} + GT\theta sin\alpha + GC\varphi sin\alpha - Gn\, nsin\alpha + M(e^{-K1Y} - U) - \frac{1}{D_a}U - Fme^{-2\lambda Y}$

$\frac{\partial \theta}{\partial t_1^*} = \frac{1}{Prnf}(1 + Rd)\frac{\partial^2 \theta}{\partial Y^2}$

$\frac{\partial \varphi}{\partial t_1^*} = \frac{1}{Sc}\frac{\partial^2 C\prime}{\partial Y^2} - Kc\varphi$

$\frac{\partial n}{\partial t_1^*} = \frac{1}{Scm}\frac{\partial^2 n}{\partial Y^2}$.

The boundary conditions becomes

For $\forall t' \le 0, U = 0, \theta = 0, \varphi = 0, n = 0$

For $t' > 0, U = 1, \theta = 1, \varphi = t_1^*, n = 1$ at $Y = 0$

At $y \to \infty, U \to 0, \theta \to 0$, $\varphi \to 0$, $n \to 0$,

Solution is:

$$U = \frac{1}{2}\left[e^{-2\eta\sqrt{\left(M+\frac{1}{D\alpha}\right)t_1^*}}erfc\left(\eta - \sqrt{\left(M+\frac{1}{D\alpha}\right)t_1^*}\right) + e^{2\eta\sqrt{\left(M+\frac{1}{D\alpha}\right)t_1^*}}erfc\left(\eta + \sqrt{\left(M+\frac{1}{D\alpha}\right)t_1^*}\right)\right] -$$

$$A\left\{\frac{e^{at_1^*}}{2}\left[e^{-2\eta\sqrt{\left(a+M+\frac{1}{D\alpha}\right)t_1^*}}erfc\left(\eta - \sqrt{\left(a+M+\frac{1}{D\alpha}\right)t_1^*}\right) + e^{2\eta\sqrt{\left(a+M+\frac{1}{D\alpha}\right)t}}erfc\left(\eta + \sqrt{\left(a+M+\frac{1}{D\alpha}\right)t_1^*}\right)\right] -\right.$$

$$\left.\frac{1}{2}\left[e^{-2\eta\sqrt{\left(M+\frac{1}{D\alpha}\right)t_1^*}}erfc\left(\eta - \sqrt{\left(M+\frac{1}{D\alpha}\right)t_1^*}\right) + e^{2\eta\sqrt{\left(M+\frac{1}{D\alpha}\right)t}}erfc\left(\eta + \sqrt{\left(M+\frac{1}{D\alpha}\right)t_1^*}\right)\right]\right\} - B\left\{\frac{e^{bt_1^*}}{2b}\left[e^{-2\eta\sqrt{\left(b+M+\frac{1}{D\alpha}\right)t_1^*}}erfc\left(\eta - \right.\right.\right.$$

$$\left.\left.\left.\sqrt{\left(b+M+\frac{1}{D\alpha}\right)t_1^*}\right) + e^{2\eta\sqrt{\left(b+M+\frac{1}{D\alpha}\right)t_1^*}}erf_c\left(\eta + \sqrt{\left(b+M+\frac{1}{D\alpha}\right)t_1^*}\right)\right] - \frac{1}{2b}\left[e^{-2\eta\sqrt{\left(M+\frac{1}{D\alpha}\right)t_1^*}}erfc\left(\eta - \sqrt{\left(M+\frac{1}{D_\alpha}\right)t_1^*}\right) +\right.\right.$$

$$\left.\left.e^{2\eta\sqrt{\left(M+\frac{1}{D\alpha}\right)t_1^*}}erfc\left(\eta + \sqrt{\left(M+\frac{1}{D\alpha}\right)t_1^*}\right)\right] - \left[\frac{1}{2}\left(t_1^* - \eta\sqrt{\frac{t_1^*}{M+\frac{1}{D\alpha}}}\right)e^{-2\eta\sqrt{\left(M+\frac{1}{D\alpha}\right)t_1^*}}erfc\left(\eta - \sqrt{\left(M+\frac{1}{D_\alpha}\right)t_1^*}\right) - \frac{1}{2}\left(t +\right.\right.\right.$$

$$\left.\left.\left.\eta\sqrt{\frac{t}{M+1/D\alpha}}\right)e^{2\eta\sqrt{\left(M+\frac{1}{D\alpha}\right)t_1^*}}erfc\left(\eta + \sqrt{\left(M+\frac{1}{D_\alpha}\right)t_1^*}\right)\right]\right\} - C\left\{\frac{e^{ct_1^*}}{2}\left[e^{-2\eta\sqrt{\left(c+M+\frac{1}{D\alpha}\right)t_1^*}}erfc\left(\eta - \sqrt{\left(c+M+\frac{1}{D\alpha}\right)t_1^*}\right) +\right.\right.$$

$$e^{2\eta\sqrt{\left(c+M+\frac{1}{D\alpha}\right)t}}erfc\left(\eta+\sqrt{\left(c+M+\frac{1}{D\alpha}\right)t_1^*}\right)\Big]-\frac{1}{2}\left[e^{-2\eta\sqrt{\left(M+\frac{1}{D\alpha}\right)t_1^*}}erfc\left(\eta-\sqrt{\left(M+\frac{1}{D\alpha}\right)t_1^*}\right)+e^{2\eta\sqrt{\left(M+\frac{1}{D\alpha}\right)t_1^*}}erfc\left(\eta+\sqrt{\left(M+\frac{1}{D\alpha}\right)t_1^*}\right)\right]\Big\}$$

$$-\frac{M}{d}\left\{\frac{e^{dt_1^*}}{2}\left[e^{-2\eta\sqrt{t_1^*\left(d+M+\frac{1}{D\alpha}\right)}}erfc\left(\eta-\sqrt{\left(d+M+\frac{1}{D\alpha}\right)t_1^*}\right)+e^{2\eta\sqrt{t_1^*\left(d+M+\frac{1}{D\alpha}\right)}}erfc\left(\eta+\sqrt{\left(d+M+\frac{1}{D\alpha}\right)t_1^*}\right)\right]-\frac{1}{2}\left[e^{-2\eta\sqrt{\left(M+\frac{1}{D\alpha}\right)t_1^*}}erfc\left(\eta-\sqrt{\left(M+\frac{1}{D\alpha}\right)t_1^*}\right)+e^{2\eta\sqrt{\left(M+\frac{1}{D\alpha}\right)t_1^*}}erfc\left(\eta+\sqrt{\left(M+\frac{1}{D\alpha}\right)t_1^*}\right)\right]\right\}$$

$$+\frac{Fm}{h}\left\{\frac{e^{ht_1^*}}{2}\left[e^{-2\eta\sqrt{\left(d+M+\frac{1}{D\alpha}\right)t_1^*}}erfc\left(\eta-\sqrt{\left(h+M+\frac{1}{D\alpha}\right)t_1^*}\right)+e^{2\eta\sqrt{\left(d+M+\frac{1}{D\alpha}\right)t_1^*}}erfc\left(\eta+\sqrt{\left(h+M+\frac{1}{D\alpha}\right)t_1^*}\right)\right]-\frac{1}{2}\left[e^{-2\eta\sqrt{\left(M+\frac{1}{D\alpha}\right)t_1^*}}erfc\left(\eta-\sqrt{\left(M+\frac{1}{D\alpha}\right)t_1^*}\right)+e^{2\eta\sqrt{\left(M+\frac{1}{D\alpha}\right)t_1^*}}erfc\left(\eta+\sqrt{\left(M+\frac{1}{D\alpha}\right)t_1^*}\right)\right]\right\}$$

$$+A\left\{\frac{e^{at_1^*}}{2}\left[e^{-2\eta\sqrt{a\frac{Prnf}{(1+Rd)}t_1^*}}erfc\left(\eta\sqrt{\frac{Prnf}{(1+Rd)}}-\sqrt{at_1^*}\right)+e^{2\eta\sqrt{a\frac{Prnf}{(1+Rd)}t_1^*}}erfc\left(\eta\sqrt{\frac{Prnf}{(1+Rd)}}+\sqrt{at_1^*}\right)\right]-erf_c\left(\eta\sqrt{\frac{Prnf}{(1+Rd)}}\right)\right\}$$

$$+B\left\{\frac{e^{bt_1^*}}{2b}\left[e^{-2\eta\sqrt{Sc}\sqrt{(b+Kc)t_1^*}}erfc\left(\eta\sqrt{Sc}-\sqrt{(b+Kc)t_1^*}\right)+e^{2\eta\sqrt{Sc}\sqrt{(b+Kc)t_1^*}}erfc\left(\eta\sqrt{Sc}+\sqrt{(b+Kc)t_1^*}\right)\right]+\frac{1}{2b}\left[e^{-2\eta\sqrt{ScKct_1^*}}erfc\left(\eta\sqrt{Sc}-\sqrt{Kct_1^*}\right)+e^{2\eta\sqrt{ScKct_1^*}}erfc\left(\eta\sqrt{Sc}-\sqrt{Kct_1^*}\right)\right]-\frac{1}{2}\left(t_1^*-\eta\sqrt{\frac{t_1^*}{ScKc}}\right)e^{-2\eta\sqrt{ScKct_1^*}}erfc\left(\sqrt{Sc}\eta-\sqrt{Kct_1^*}\right)-\frac{1}{2}\left(t_1^*+\eta\sqrt{\frac{t_1^*}{ScKc}}\right)e^{2\eta\sqrt{ScKct_1^*}}erfc\left(\sqrt{Sc}\eta+\sqrt{Kct_1^*}\right)\right\}$$

$$+C\left\{\frac{e^{ct_1^*}}{2}\left[e^{-2\eta\sqrt{cScmt_1^*}}erfc\left(\eta\sqrt{Scm}-\sqrt{ct_1^*}\right)+e^{2\eta\sqrt{cScmt_1^*}}erfc\left(\eta\sqrt{Scm}+\sqrt{ct_1^*}\right)\right]-\left[erfc\left(\eta\sqrt{Scm}\right)\right]\right\}+\frac{M}{d}e^{-2\eta K1\sqrt{t}}\left(e^{dt_1^*}-1\right)-\frac{Fm}{h}e^{-4\eta\lambda\sqrt{t}}\left(e^{ht_1^*}-1\right)$$

$$\varphi=\frac{1}{2}\left(t_1^*-\eta\sqrt{\frac{t_1^*}{ScKc}}\right)e^{-2\eta\sqrt{ScKct_1^*}}erfc\left(\sqrt{Sc}\eta-\sqrt{Kct_1^*}\right)+\frac{1}{2}\left(t_1^*+\eta\sqrt{\frac{t_1^*}{ScKc}}\right)e^{2\eta\sqrt{ScKct_1^*}}erfc\left(\sqrt{Sc}\eta+\sqrt{Kct_1^*}\right)$$

$$\theta=erfc\left(\sqrt{\frac{Prnf}{1+Rd}}\eta\right)$$

$$n=erfc\left(\sqrt{Scm}\,\eta\right),$$

where $a=\frac{(D\alpha M+1)(1+Rd)}{D\alpha(Prnf-1-Rd)}$, $b=\frac{D\alpha ScKc-MD_\alpha-1}{D\alpha(1-Sc)}$, $c=\frac{D\alpha M+1}{D\alpha(Scm-1)}$, $d=K1^2-M-\frac{1}{D\alpha}$, $h=4\lambda^2-M-\frac{1}{D\alpha}$

$A=\frac{GTsin\alpha(1+R_d)}{a(1+Rd-Prnf)}$, $B=\frac{GCsin\alpha}{b(1-Sc)}$, $C=\frac{Gnsin\alpha}{c(Scm-1)}$.

3. Results and Discussion

This section presents Laplace transform analytical solutions for unsteady ferro-nanofluid "flow across an inclined Riga plate. The regulating dimensionless parameter affects velocity, temperature, concentration, and motile microbe density distributions. Graphs indicate how electromagnetic forcing, tilt, magnetization, associated heat and mass transfer" mechanisms affect "boundary layer structure."

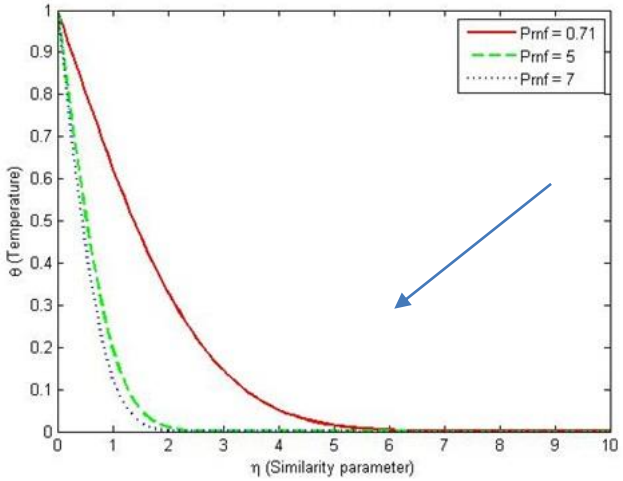

Figure 1: Temperature profile for different values of Prandtl number.

Fig.1 implies temperature profile deviation for distinct Prandtl numbers. "Increased Prandtl number" lowers temperature and thins thermal boundary layer. Larger Prandtl numbers diminish thermal diffusivity, weakening heat

diffusion away from the plate and rapid fluid temperature depreciation.

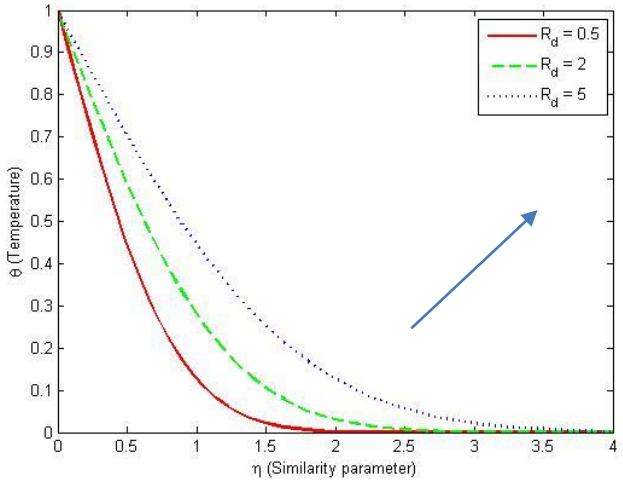

Figure 2: Temperature profile for different values of radiation parameter.

In Fig. 2, "radiation parameter Rd" affects temperature profile. "Temperature profile and thermal boundary layer thickness" increase as radiation parameter increases. Radiation's contribution to energy equation shows that radiative heat transfer dominates conductive diffusion.

.

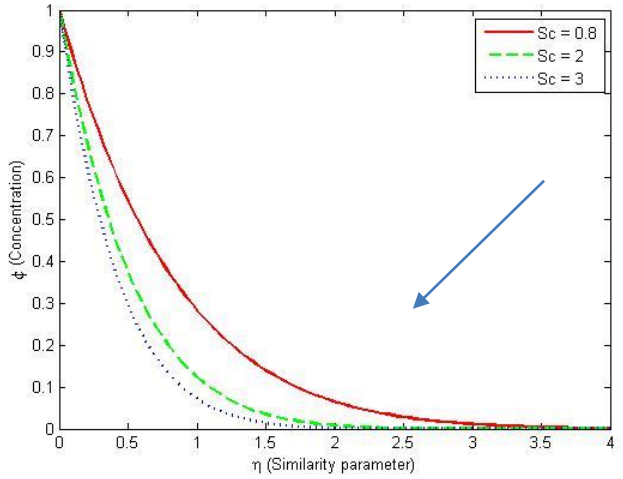

Figure 3: Concentration profile for different values of Sc.

Fig. 3 shows the "concentration profile" for distinct Schmidt numbers, Sc. As Sc increases, the concentration curve attenuates and reduces boundary layer thickness and mass diffusivity. As in analytical solution, higher Sc values increase concentration exponential decay and surface mass transfer rate.

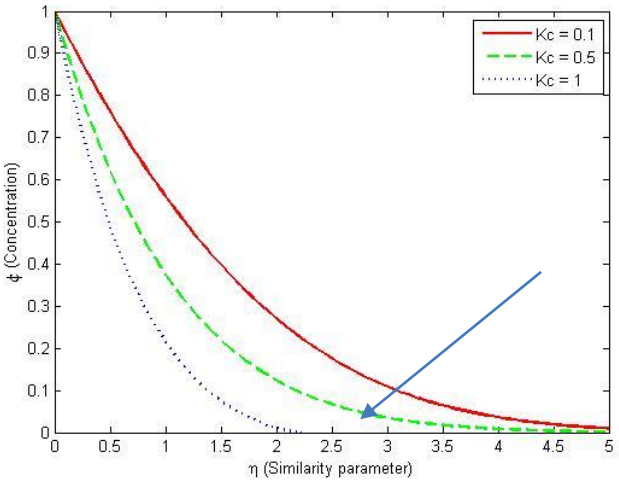

Figure 4: Concentration profile for different values of chemical reaction parameter.

Fig. 4 shows the concentration profile for "distinct Kc values." As Kc increases, concentration distribution reduces monotonically. In the boundary layer, species concentration is suppressed. Higher chemical reaction parameter Kc contracts "solutal boundary layer."

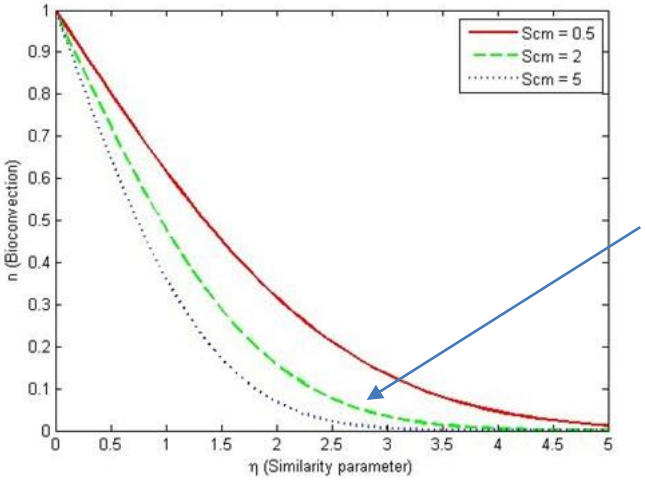

Figure 5: Bioconvection profile for different values of bioconvective Schmidt number.

Impact of bioconvection "Schmidt number Scm" over bioconvection profile is illustrated in Fig.5. The bioconvection profiles reveal that increasing Scm significantly suppresses the motile microorganism density within boundary layer. Larger values of Scm subsides the microorganism diffusivity, that restricts their migration away from surface and results in a thinner bioconvective boundary layer.

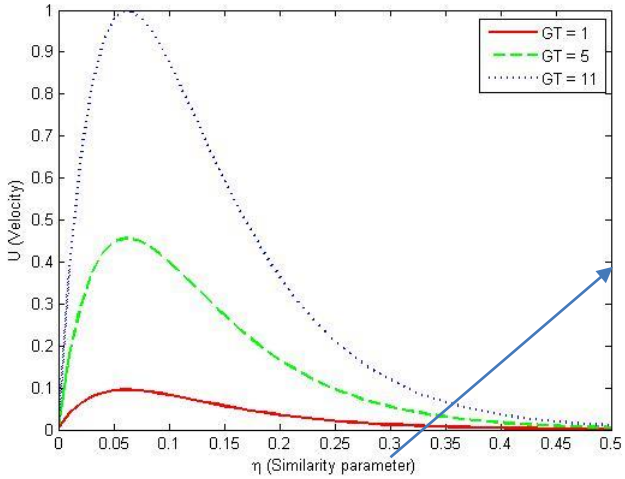

Figure 6: Velocity profile for different values of thermal Grashof number.

Fig. 6 shows velocity profiles for distinct thermal granhof numbers, GT. Increased thermal Grashof number improves velocity profile, with a peak near wall due to thermal buoyancy. Additionally, when GT rises, the momentum boundary layer contracts, indicating a more restricted flow structure.

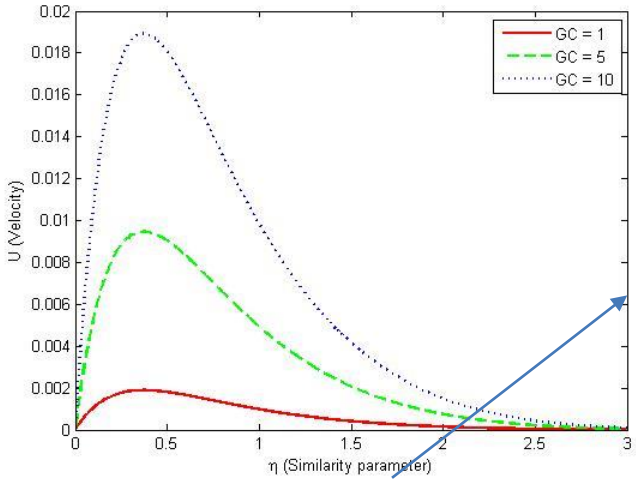

Figure 7: Velocity profile for different values of thermal Grashof number.

Fig. 7 shows velocity profile effects for distinct "thermal Grashof numbers." The boundary layer velocity increases significantly as GC increases due to significant solutal buoyant forces. Peak velocity shifts toward the wall due to this improvement.

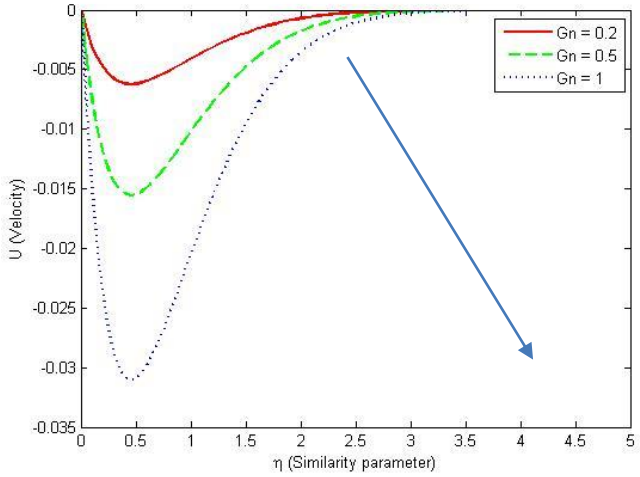

Figure 8: Velocity profile for different values of thermal Grashof number.

Bioconvection velocity profile at varied values. Figure 8 explains "Grashof number." As GN increases, flow structure changes considerably. Higher values of GN amplify the bioconvective buoyancy force generated by motile microorganisms, leading to an increase in negative velocity near the surface. This behavior signifies stronger flow retardation and the occurrence of velocity reversal within the boundary layer. GN is crucial to biconvective effects and momentum transfer in flow.

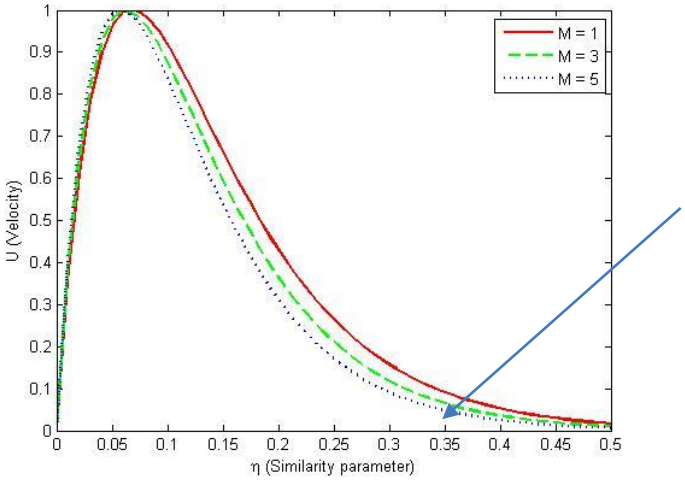

Figure 9: Velocity profile for different values of magnetic parameter.

Fig. 9 shows velocity profiles for varied magnetic parameter M values. Magnetic parameter M rises, ferro-nanofluid velocity decreases in boundary layer. "Higher M values" reduce velocity magnitude, strengthening the Lorentz force. Thus, increasing M reduces peak velocity and momentum boundary layer.

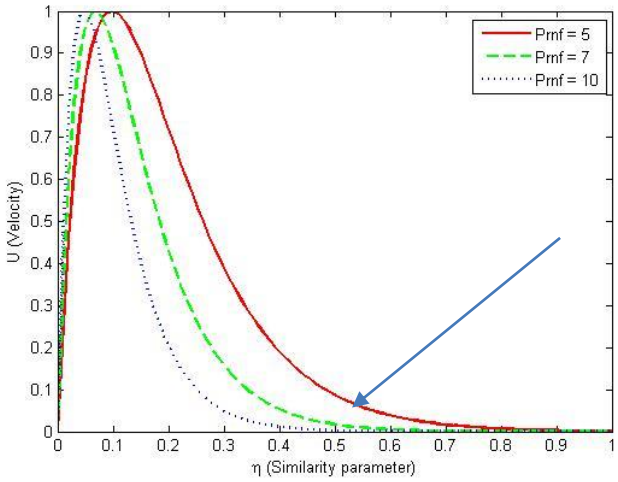

Figure 10: Velocity profile for different values of Prandtl number.

Fig. 10 displays "velocity profile" for distinct Prandtl number Prnf values. Velocity profile shows, within the boundary layer, an increased Prandtl number deteriorates the ferro-nanofluid velocity. Also, higher Prnf attenuates the thermal diffusion and thereby drops the buoyancy drive flow. As a result, the peak velocity drops and shifts closer to the surface.

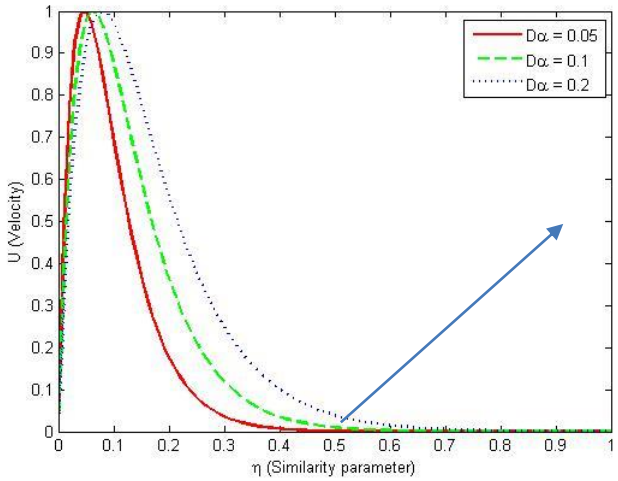

Figure 11: Velocity profile for different values of Porosity parameter.

Fig. 11 demonstrates "velocity profile" for distinct porosity parameters D*a*. Increasing D*a* increases boundary layer fluid velocity. Higher porosity reduces porous medium resistance, allowing fluid to flow more freely. With increased porosity, peak momentum and velocity boundary layer thickness rise, improving momentum conveyance.

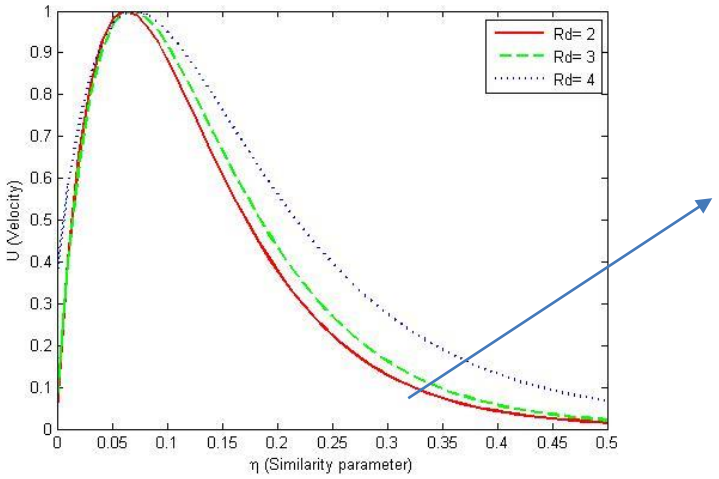

Figure 12: Velocity for different values of thermal radiation.

"Velocity profile" for distinct thermal radiation Rd values is shown in Figure 12. It is noted that increasing Rd significantly escalates the ferro-nanofluid velocity. Higher radiation intensifies thermal energy transport, thereby strengthening buoyancy forces accelerated flow. Thus, increased Rd increases peak velocity and momentum boundary layer thickness, highlighting crucial role of thermal radiation in ferro-nanofluid flow behavior.

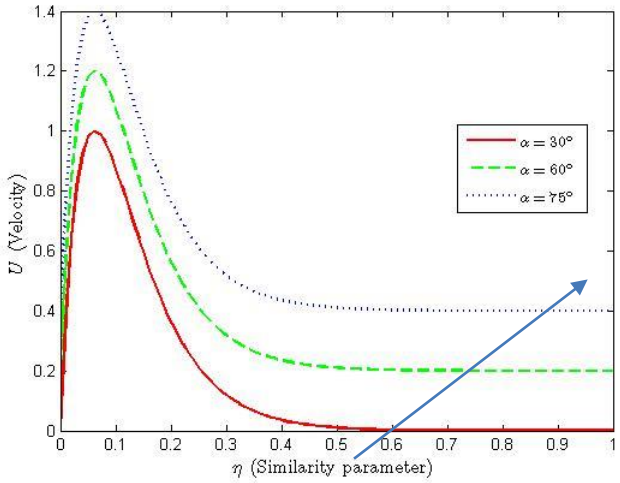

Figure 13: Velocity profile for different values of inclination.

Fig. 13 demonstrates "velocity profiles" at distinct angles of inclination (α). Increasing plate inclination increases buoyancy force at the surface, leading to higher velocities and delayed velocity profile decay. Thus, the momentum boundary layer thickens, proving that plate inclination improves ferro-nanofluid flow.

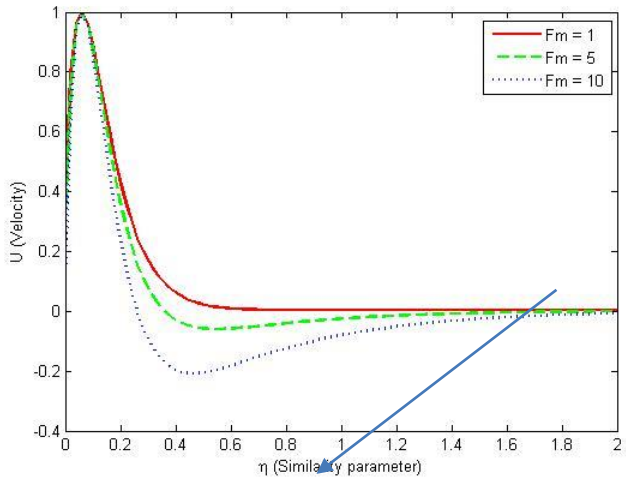

Figure 14: Velocity profile for different values of Ferrohydrodynamic parameter.

Figure 14 shows how ferrohydrodynamic parameter Fm affects velocity distribution. Increasing Fm significantly reduces the velocity due to amplified magnetic body forces and megnetoviscous effects. At sufficiently large Fm, flow reversal is observed, confirming the dominance of magnetic forces over inertia.

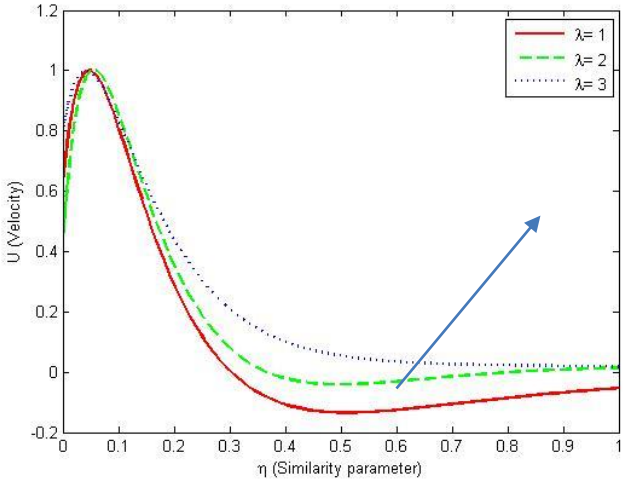

Figure 15: Velocity profile for different values of Spatial decay parameter.

Fig. 15 displays impact of spatial decay parameter λ on velocity profile. An increase in λ strengthens near-wall magnetic forcing while limiting its penetration depth, owing to the exponential decay of the applied magnetic field. This localized enhancement accelerates the flow and significantly diminishes flow reversal.

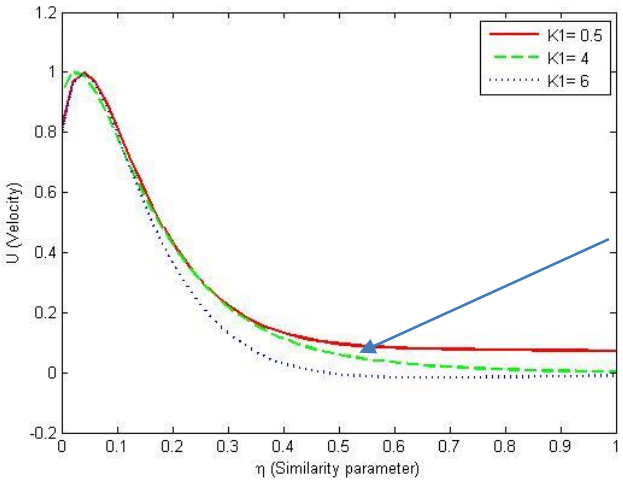

Figure 16: Velocity profile for different values of electromagnetic Spatial decay parameter.

"Velocity distribution" is affected by the electromagnetic spatial decay parameter K1 in Figure 16. Increasing K1 significantly reduces boundary layer velocity. Physically, larger values of K1 correspond to a more rapid attenuation of the Lorentz force away from the Riga plate, thereby restricting electromagnetic momentum transfer to the near-wall region. Consequently, the flow experiences weaker electromagnetic acceleration and stronger damping, resulting in a faster decay of the "velocity profile."

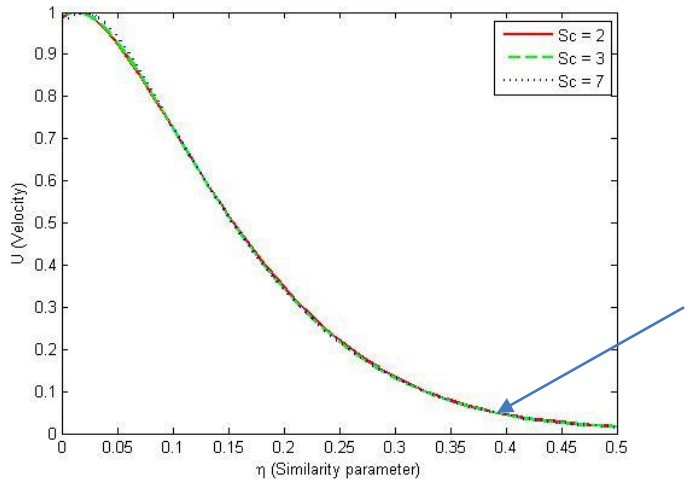

Figure 17: Velocity profile for different values Schmidt number.

Figure 17 depicts "Schmidt number Sc's" impact on velocity distribution. For example, increasing Sc reduces velocity near the plate. Due to decreased mass diffusivity, larger Sc values weaken the momentum equation's solutal buoyant force. Far from the surface, concentration gradients diminish, and all velocity profiles asymptotically merge.

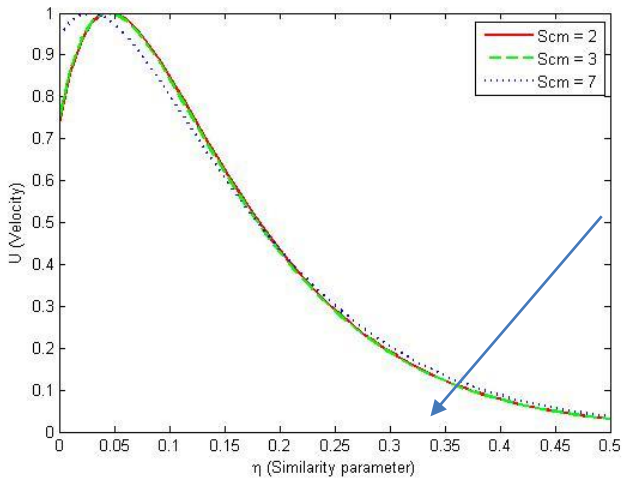

Figure 18: Velocity profile for different values of bioconvective Schmidt number.

Figure 18 shows "velocity patterns" for distinct bioconvective Schmidt numbers Scm. As Scm increases, velocity magnitude decreases slightly. Velocity peaks near the plate and decays monotonically with similarity variable for all Scm values.

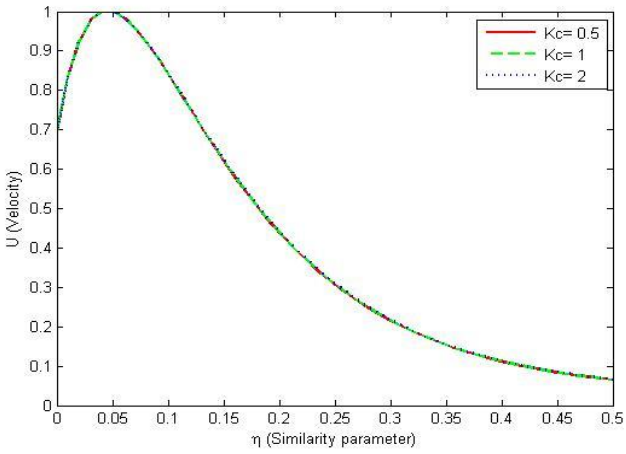

Figure 19: Velocity profile for different values of chemical reaction parameter.

"Velocity patterns" match for varied chemical reaction parameter Kc values in Figure 19. This behavior is expected since Kc appears only in the concentration equation and does not directly enter the momentum equation. Variations in chemical reaction strength affect concentration field but not velocity dispersion.

4. Conclusions

Overall, result reveals that

- Increasing Prnf lowers ferro-nano fluid temperature.
- Improved "Schmidt number and chemical reaction parameters" reduce concentration profile.
- High bioconvective Schmidt number inhibits bioconvection.
- Enhanced values of $GT, GC, \alpha, D\alpha, \lambda$ and S_c intensify the velocity profile, whereas increased values of Gn, Prnf, $Rd, M, Fm, K1$ and Scm decelerate the velocity profile.
- The results demonstrate that ferro-nanofluids offer a highly controllable flow platform, when velocity can be selectively enhanced or suppressed by tuning thermal, magnetic, and nanoparticle parameters, making them ideal for smart thermal, biomedical and magneto fluidic applications.

Nomenclature

$u \rightarrow$ "velocity component along x direction. $\alpha \rightarrow$ Inclination of the plate with the vertical $\rho_{nf} \rightarrow$ Density of the ferro-nano fluid(kg/m^3) $\vartheta_{nf} \rightarrow$ Kinematic Viscosity coefficient of nano fluid(m^2/s) $\mu_{nf} \rightarrow$ Dynamic Viscosity of the ferro-nanofluid(Pa.s) $g \rightarrow$ Acceleration due to gravity(m/s^2) $\beta_1 \rightarrow$ Thermal volumetric expansion coefficient(1/Kelvin) $\beta_2 \rightarrow$ Solutal expansion coefficient (m^3/Kg) $\beta_3 \rightarrow$ Bioconvection buoyancy coefficient (m^3) $C_p \rightarrow$ Specific heat capacity $K \rightarrow$ Thermal Conductivity $\sigma^* \rightarrow$ Stefan-Boltzmann Number $B_0 \rightarrow$ Uniform Magnetic field (tesla) $\rho \rightarrow$ Fluid's density $\mu_0 \rightarrow$ Magnetic permeability of free space (H/m) $\rightarrow$Temperature of the nano fluid(Kelvin) C$\rightarrow$ Concentration of the nanoparticle (Kg/m^3) N$\rightarrow$ Motile microorganism density (m^{-3})	T $\sigma \rightarrow$ Eelectrical conductivity of he ferro-nano fluid (S/m) $T_\infty \rightarrow$ Ambient Temperature (Kelvin) $C_\infty \rightarrow$ Ambient Nanoparticles concentration $N_\infty \rightarrow$ Ambient microorganism density. $T_W \rightarrow$ Wall Temperature (Kelvin) $C_W \rightarrow$ Wall Nanoparticles concentration $N_W \rightarrow$ Wall microorganism density $u_0 \rightarrow$ Induced streaming velocity from Riga plate. (m/s) $H_0 \rightarrow$ Magnetic field intensity(A/m) $\lambda \rightarrow$ Spatial decay parameter (1/m) $K^* \rightarrow$ Permeability of the porous medium (m^2) $k_{nf} \rightarrow$ Thermal conductivity of the ferro-nano fluid (W/m-K) $C_{p,nf} \rightarrow$ Specific heat at constant pressure of the ferro-nanofluid (J/kg.K) $D_{nf} \rightarrow$ Mass diffusion coefficient (m^2/s) $k_t \rightarrow$ First order chemical reaction rate constant (1/s) $D_m \rightarrow$ Microorganism diffusion coefficient. (m^2/s) $K1 \rightarrow$ Electromagnetic Spatial Decay Parameter(1/m)"

Authors' contributions

The author read and approved the final manuscript.

Conflicts of interest

The author declares no conflict of interest.

Funding

This research received no external funding.

Data availability

No new data were created.

References

[1] A. Selvaraj, S.D. Jose, R. Muthucumaraswamy, S. Karthikeyan, MHD parabolic flow past an accelerated isothermal vertical plate with heat and mass diffusion in the presence of rotation, *Mater. Today Proc.* **46** (2021) 3546–3549.

[2] D. Lakshmikaanth, A. Selvaraj, P. Selvaraju, S.D. Jose, Hall and heat source effects of flow past a parabolic accelerated isothermal vertical plate in the presence of chemical reaction and radiation, *JP J. Heat Mass Transfer* **34** (2023) 105–126.

[3] D.C. Kesavaiah, R.S. Jahagirdar, Radiation absorption and chemical reaction effects on MHD flow through porous medium past an exponentially accelerated inclined plate, *Int. J. Res. Appl. Sci. Eng. Technol*. **6** (2018) 1370–1381.
[4] B.P. Reddy, M.H. Simba, A. Hugo, Effects of thermo-diffusion and chemical reaction on MHD radiated unsteady flow past an exponentially accelerated inclined permeable plate embedded in a porous medium, *Int. J. Chem. Eng*. (2023).
[5] M.V. Krishna, N.A. Ameer, A.J. Chamkha, Radiation absorption on MHD convective flow of nanofluids through a vertically travelling absorbent plate, *Ain Shams Eng. J*. **12** (2021) 3043–3056.
[6] S. Das, R.N. Jana, O.D. Makinde, Transient natural convection in a vertical channel filled with nanofluids in the presence of thermal radiation, *Alex. Eng. J*. **55** (2016) 253–262.
[7] P.D. Prasad, R.V.M.S.S.K. Kumar, S.V.K. Varma, Heat and mass transfer analysis for the MHD flow of nanofluid with radiation absorption, *Ain Shams Eng. J*. **9** (2018) 801–813.
[8] S. Agarwalla, N. Ahmed, MHD mass transfer flow past an inclined plate with variable temperature and plate velocity embedded in a porous medium, *Heat Transfer Asian Res.* **47** (2018) 27–41.
[9] M.V. Krishna, A.J. Chamkha, Hall effects on MHD squeezing flow of a water-based nanofluid between two parallel disks, *J. Porous Media* 22 (2019).
[10] T. Hayat, T. Abbas, M. Ayub, M. Farooq, A. Alsaedi, Flow of nanofluid due to convectively heated Riga plate with variable thickness, *J. Mol. Liq.* **222** (2016) 854–862.
[11] J. Prakash, A. Selvaraj, P. Ragupathi, Q.M. Al-Mdallal, S. Saranya, Thermal and radiative effects on unsteady MHD flow of Casson fluid past a rotating porous medium with variable mass diffusion, *Case Stud. Therm. Eng*. (2025). https://doi.org/10.1016/j.csite.2025.105865.
[12] K. Raghunath, R.M. Ramana, V.R. Reddy, M. Obulesu, Diffusion-thermo and chemical reaction effects on MHD Jeffrey nanofluid over an inclined vertical plate, *J. Nanofluids* **12** (2023) 147–156.
[13] M. Afridi, M. Qasim, A. Hussanan, Second law analysis of dissipative flow over a Riga plate with nonlinear Rosseland thermal radiation, *Entropy* **20** (2018) 615.
[14] B.P. Reddy, J.A. Rao, Radiation and thermal diffusion effects on an unsteady MHD free convection mass transfer flow, *J. Eng. Phys. Thermophys*. **84** (2011) 1369–1378.
[15] S. Rana, R. Tabassum, R. Mehmood, E.M. Tag-Eldin, R. Shah, Influence of Hall current and Lorentz force in an inclined slip flow of couple stress fluid over a Riga plate, *Ain Shams Eng. J*. (2023).
[16] E.M. Arthur, I.Y. Seini, L.B. Bortteir, Analysis of Casson fluid flow over a vertical porous surface with chemical reaction, *J. Appl. Math. Phys*. **3** (2015) 713–723.
[17] J. Wang et al., Computational analysis for bioconvection of microorganisms in Prandtl nanofluid Darcy–Forchheimer flow, *Nanomaterials* **12** (2022) 1791.
[18] U. Farooq, T. Liu, U. Farooq, S. Majeed, Non-similar analysis of bioconvection MHD micropolar nanofluid (2024). https://doi.org/10.1007/s13201-024-02143-0.
[19] F. Wang et al., Unsteady micropolar nanofluid flow over an exponentially stretching curved surface, Waves Random Complex Media (2024).
[20] K.K. Asogwa, F. Mebarek-Oudina, I.L. Animasaun, Comparative investigation of radiative Riga plate heat transport, *Arab. J. Sci. Eng*. **47** (2022) 8721–8738.
[21] R. Vemula, L. Debnath, S. Chakrala, Unsteady MHD free convection nanofluid flow, *Int. J. Appl. Comput. Math*. **3** (2017) 1271–1287.
[22] S.M. Hussain et al., Thermal radiation impact on magnetonanofluid flow, *Int. J. Heat Technol*. **36** (2018) 1163–1173.
[23] S. Bilal et al., Analytical treatment of radiative Casson fluid over an inclined Riga surface, *Alex. Eng. J*. **60** (2021) 4243–4253.
[24] N. Abbas, S. Nadeem, A. Issakhov, Transportation of modified nanofluid over a Riga plate, *Ain Shams Eng. J*. (2021).
[25] K. Das, P.R. Durai, P.K. Kundu, Nanofluid bioconvection with chemical reaction, *J. Mech. Sci. Technol*. **29** (2015) 4841–4849.
[26] K. Swain et al., Influence of MWCNT/Fe_3O_4 hybrid nanoparticles, *J. Therm. Anal. Calorim*. (2021).
[27] M.M. Bhatti, E.E. Michaelides, Arrhenius activation energy on thermo-bioconvection nanofluid flow over a Riga plate, *J. Therm. Anal. Calorim*. **143** (2021) 2029–2038.
[28] A.J. Chamkha, A.M. Aly, MHD free convection flow of a nanofluid, *Chem. Eng. Commun*. **198** (2011) 425–441.
[29] A. Shahid et al., Numerical investigation on swimming of gyrotactic microorganisms, *Mathematics* **8** (2020) 380.
[30] S. Das, R.N. Jana, Natural convective magnetonanofluid flow, *Alex. Eng. J*. **54** (2015) 55–64.
[31] M.M. Bhatti et al., MHD nanofluid flow with gyrotactic microorganisms, *Neural Comput. Appl*. **30** (2018) 1237–1249.
[32] K. Hosseinzadeh et al., Nano-bioconvective fluid flow with MHD, *Inform. Med. Unlocked* **21** (2020) 100462.
[33] R. Ganesan et al., Chemical reaction effects on unsteady MHD Casson fluid flow, *J. Adv. Res. Fluid Mech. Therm. Sci*. **133** (2025) 24–36.
[34] D. Lakshmikaanth, A. Selvaraj, S. Bhavani, Exploration of Hall and Dufour effects on parabolic flow, *CFD Lett*. **17** (2025) 60–77.
[35] S. Rosseland, Astrophysik and Atom-Theoretische Grundlagen, Springer, Berlin, Germany (1931).